Numerical Solution of 2D Darcy Flow with Full-Tensor Conductivity Using Mimetic Differences Nodes

Dalston J. Karto and Miguel A. Dumett

May 4, 2026

Publication Number: CSRCR2026-02

Computational Science & Engineering Faculty and Students Research Articles

Database Powered by the Computational Science Research Center Computing Group & Visualization Lab

COMPUTATIONAL SCIENCE & ENGINEERING

SAN DIEGO STATE UNIVERSITY

Computational Science Research Center
College of Sciences
5500 Campanile Drive
San Diego, CA 92182-1245
(619) 594-3430

Numerical Solution of 2D Darcy Flow with Full-Tensor Conductivity Using Mimetic Differences

Dalston J. Karto* Miguel A. Dumett‡

May 4, 2026

Abstract

In this work, we document the numerical solution of a two-dimensional Darcy equation with heterogeneous anisotropic full-tensor conductivity using mimetic difference operators from the MOLE library in MATLAB. A manufactured exact solution is used to derive the forcing term and Dirichlet boundary data. Special care is required in the discrete treatment of mixed tensor terms because u_x and u_y are stored on different staggered faces. After correcting for this tensor assembly, numerical experiments for $\alpha = 1, 10^2, 10^3$ show stable solutions and approximately fourth-order decay in the reported l_2 errors under mesh refinement.

1 Introduction

The Darcy equation models steady-state flow in porous media and appears in applications involving groundwater flow and petroleum engineering [5]. The model obeys Darcy's law in how flux relates to pressure gradient through a conductivity tensor. When the porous media is anisotropic and spatially varying, conductivity becomes a full tensor rather than a scalar, and numerical treatment becomes more delicate.

In two spatial dimensions, anisotropic Darcy flow can be written as an elliptic equation in divergence form. When tensor is full, each component of flux depends on more than one component of gradient. This creates additional complexity in a staggered-grid mimetic framework because horizontal and vertical gradient components are stored on different families of faces.

This work implements a numerical solver for a two-dimensional Darcy equation with heterogeneous full-tensor conductivity using MOLE, following the benchmark test problem reported by Traverso et al [5]. The implementation is verified by means of a manufactured exact solution, and compares convergence behavior across several values of the anisotropy parameter α.

*Computational Science Master Program at San Diego State University (dkarto7361@sdsu.edu).

†Editor: Jose E. Castillo.

‡Computational Science Research Center at San Diego State University (mdumett@sdsu.edu).

2 Mathematical Formulation

2.1 Governing Equation and Domain

Let $\Omega = [0,1] \times [0,1]$. The scalar potential head u(x,y) satisfies

$$-\nabla \cdot \big(C(x,y)\nabla u(x,y)\big) = f(x,y), \qquad (x,y) \in \Omega. \tag{1}$$

In this report, the Darcy flux is defined by

$$q = -C\nabla u, \tag{2}$$

so that the scalar equation takes the form (1).

2.2 Boundary Condition

Dirichlet boundary conditions are imposed on all four sides of the domain using the manufactured exact solution:

$$u(x,y) = u_{\text{exact}}(x,y), \qquad (x,y) \in \partial\Omega \tag{3}$$

2.3 Conductivity Tensor

The heterogeneous anisotropic conductivity tensor is given by:

$$C(x,y) = \begin{bmatrix} y^2 + \alpha x^2 & (\alpha-1)xy \\ (\alpha-1)xy & x^2 + \alpha y^2 \end{bmatrix} \tag{4}$$

The parameter α controls the degree of anisotropy. When $\alpha = 1$, the off-diagonal terms vanish and the tensor becomes diagonal. When $\alpha > 1$, the tensor becomes anisotropic and the mixed terms become active. The coupling between the x-faces and the y-faces must be handled correctly.

2.4 Manufactured exact solution

We introduce the manufactured exact solution that was used for verifying the implementation

$$u_{\text{exact}}(x,y) = \exp\left(-20\pi\left(\left(x - \frac{1}{2}\right)^2 + \left(y - \frac{1}{2}\right)^2 \right) \right) \tag{5}$$

2.5 Derivation of forcing term

We obtain the forcing term by substituting the exact solution into the operator.

$$f = -\nabla \cdot (C\nabla u) \tag{6}$$

Expanding the divergence gives

$$f = -\left[\frac{\partial}{\partial x}(C_{11}u_x + C_{12}u_y) + \frac{\partial}{\partial y}(C_{21}u_x + C_{22}u_y) \right] \tag{7}$$

All derivatives of the manufactured solution are evaluated analytically in MATLAB and used to construct the right-hand side pointwise.

3 Mimetic Discretization

3.1 Grid Layout

The domain is discretized using a uniform mesh with m cells in the x-direction and n cells in the y-direction. The grid spacings are

$$dx = \frac{1}{m}, \qquad dy = \frac{1}{n}.$$

The scalar unknown u is stored at cell centers $(x_{i+\frac{1}{2}}, y_{j+\frac{1}{2}})$. The flux component q_x and derivative u_x are stored on x-faces $(x_i, y_{j+\frac{1}{2}})$, while q_y and u_y are stored on y-faces $(x_{i+\frac{1}{2}}, y_j)$. This staggered placement is essential because the off-diagonal tensor terms couple variables from different face families.

3.2 Mimetic Gradient and Divergence Operators

The MOLE library is used to generate the mimetic gradient and divergence operators [3, 4]::

$$G = \texttt{grad2D}(k, m, dx, n, dy), \qquad D = \texttt{div2D}(k, m, dx, n, dy). \tag{8}$$

The gradient operator maps cell-centered scalar values to face-based derivatives, and the divergence maps face-based flux values back to cell centers. Following the mimetic flux-divergence construction [1, 2], the discrete elliptic operator is assembled as

$$L = -DKG, \tag{9}$$

where K is the block tensor operator acting on the face-based gradient vector.

3.3 Tensor Sampling on Faces

Because the conductivity tensor acts on face quantities, its components must be evaluated at the correct face locations.

For x-faces, the relevant coordinates are

$$(x_i, y_{j+\frac{1}{2}}),$$

so

$$C^F_{11} = y^2 + \alpha x^2 \quad \text{evaluated on x-faces,} \tag{10}$$

$$C^F_{12,x} = (\alpha - 1)xy \quad \text{evaluated on x-faces.} \tag{11}$$

For y-faces, the relevant coordinates are

$$(x_{i+\frac{1}{2}}, y_j),$$

so

$$C^F_{22} = x^2 + \alpha y^2 \quad \text{evaluated on y-faces,} \tag{12}$$

$$C^F_{12,y} = (\alpha - 1)xy \quad \text{evaluated on y-faces.} \tag{13}$$

This produces separate arrays for the x-face and y-face tensor values.

3.4 Mixed Tensor Terms and Face Transfer

The diagonal tensor terms are straightforward: C_{11} multiplies u_x on x-faces, and C_{22} multiplies u_y on y-faces. The off-diagonal terms are more delicate because q_x depends on u_y and q_y depends on u_x. Since these derivatives are not collocated on the grid, a naive diagonal treatment of K_{12} and K_{21} is invalid.

To account for this, transfer operators are introduced:

$$I_{y\to x} = C_{x\to x} F_{y\to c}, \qquad I_{x\to y} = C_{y\to y} F_{x\to c}. \tag{14}$$

These operators move data between the two face families through a center representation before multiplication by the corresponding tensor coefficients.

3.5 Block Tensor Construction

The block conductivity operator is

$$K = \begin{bmatrix} K_{11} & K_{12} \\ K_{21} & K_{22} \end{bmatrix}, \tag{15}$$

with

$$K_{11} = \mathrm{diag}(C_{11}^F), \tag{16}$$
$$K_{12} = \mathrm{diag}(C_{12,x}^F)\, I_{y\to x}, \tag{17}$$
$$K_{21} = \mathrm{diag}(C_{12,y}^F)\, I_{x\to y}, \tag{18}$$
$$K_{22} = \mathrm{diag}(C_{22}^F). \tag{19}$$

This is the discrete analog of

$$\begin{bmatrix} q_x \\ q_y \end{bmatrix} = - \begin{bmatrix} C_{11} & C_{12} \\ C_{21} & C_{22} \end{bmatrix} \begin{bmatrix} u_x \\ u_y \end{bmatrix}. \tag{20}$$

3.6 Boundary Treatment

Dirichlet boundary conditions are imposed using the exact solution evaluated on the boundary. In the implementation, MOLE's scalar boundary condition utility

`addScalarBC2D`

is used to form a modified system

$$L_0 u^h = F_0, \tag{21}$$

which is then solved directly.

4 Numerical Algorithm

The computational procedure can be summarized as follows:

1. Choose mesh sizes m, n and anisotropy parameter α.

2. Construct the uniform cell-centered and staggered face grids.
3. Evaluate the manufactured exact solution and the boundary data.
4. Compute tensor coefficients on x-faces and y-faces.
5. Build the mimetic gradient and divergence operators using MOLE.
6. Construct interpolation operators used in the mixed tensor coupling.
7. Assemble the block conductivity matrix K.
8. Construct the forcing term from the exact solution and tensor derivatives.
9. Form the discrete operator $L = -DKG$.
10. Impose Dirichlet boundary conditions using `addScalarBC2D`.
11. Solve the resulting linear system for the numerical potential u^h.
12. Recover numerical fluxes and compare them to exact fluxes.
13. Compute the l^2 errors, convergence rates, and extrema.
14. Repeat for several mesh resolutions and values of α.

5 Numerical Results

Numerical experiments were performed for several mesh resolutions and for $\alpha = 1, 10^2$, and 10^3. The manufactured solution was used throughout so that both the scalar potential and the flux components could be compared directly with their exact values.

Tables 1, 2, and 3 report representative error norms for the scalar solution for $\alpha = 1$, $\alpha = 10$, and $\alpha = 100$. In all cases, the error decreases rapidly as the mesh is refined.

5.1 Convergence of the Scalar Solution

For all three anisotropy values, the reported errors decrease monotonically with mesh refinement. The error constants increase with α, as expected, because stronger anisotropy makes the mixed tensor coupling more demanding numerically. However, no loss of stability is observed, and the measured rates approach four on the finest meshes for both the scalar solution and the flux components.

5.2 Approximate and Exact Solution Plots

Figures 1–3 show the approximate solution, the manufactured exact solution, and the pointwise error for a representative anisotropy value. At the plotted scale, the numerical and exact contours are visually almost indistinguishable. The error field is smooth, localized, and small in magnitude, which is consistent with the quantitative convergence data reported in the tables.

The contour plots show close agreement between the numerical and exact solutions, especially on refined meshes. The error field remains small and smooth, with largest magnitude concentrated near the interior region where the solution gradients are strongest.

Table 1: l^2-norms of the error for the Darcy test problem, $\alpha = 1$.

h	$\|u - u^h\|_{l^2}$	Rate	$\|q_x - q_x^h\|_{l^2}$	Rate	$\|q_y - q_y^h\|_{l^2}$	Rate	$u_{\min}$	$u_{\max}$
1/16	6.802e-03	—	5.09E-03	—	5.09E-03	—	2.27E-14	8.92E-01
1/32	4.511e-04	3.91	3.43E-04	3.89	3.43E-04	3.89	2.27E-14	9.70E-01
1/64	2.883e-05	3.97	2.20E-05	3.96	2.20E-05	3.96	2.27E-14	9.92E-01
1/128	1.813e-06	3.99	1.39E-06	3.99	1.39E-06	3.99	2.27E-14	9.98E-01
1/256	1.135e-07	4	8.69E-08	4	8.69E-08	4	2.27E-14	1.00E+00

Table 2: l^2-norms of the error for the Darcy test problem, $\alpha = 10^2$.

h	$\|u - u^h\|_{l^2}$	Rate	$\|q_x - q_x^h\|_{l^2}$	Rate	$\|q_y - q_y^h\|_{l^2}$	Rate	$u_{\min}$	$u_{\max}$
1/16	4.005e-02	—	1.59E+00	—	1.59E+00	—	-5.37E-03	8.78E-01
1/32	4.969e-03	3.01	1.59E-01	3.32	1.59E-01	3.32	-1.08E-03	9.67E-01
1/64	3.825e-04	3.7	1.12E-02	3.83	1.12E-02	3.83	-1.06E-04	9.92E-01
1/128	2.485e-05	3.94	7.11E-04	3.97	7.11E-04	3.97	-6.81E-06	9.98E-01
1/256	1.562e-06	3.99	4.45E-05	4	4.45E-05	4	-3.68E-07	1.00E+00

Table 3: l^2-norms of the error for the Darcy test problem, $\alpha = 10^3$.

h	$\|u - u^h\|_{l^2}$	Rate	$\|q_x - q_x^h\|_{l^2}$	Rate	$\|q_y - q_y^h\|_{l^2}$	Rate	$u_{\min}$	$u_{\max}$
1/16	4.618e-02	—	1.73E+01	—	1.73E+01	—	-7.17E-03	8.75E-01
1/32	6.786e-03	2.77	1.99E+00	3.12	1.99E+00	3.12	-1.76E-03	9.66E-01
1/64	6.199e-04	3.45	1.57E-01	3.67	1.57E-01	3.67	-2.49E-04	9.92E-01
1/128	4.435e-05	3.81	1.04E-02	3.91	1.04E-02	3.91	-2.26E-05	9.98E-01
1/256	2.889e-06	3.94	6.60E-04	3.98	6.60E-04	3.98	-1.61E-06	1.00E+00

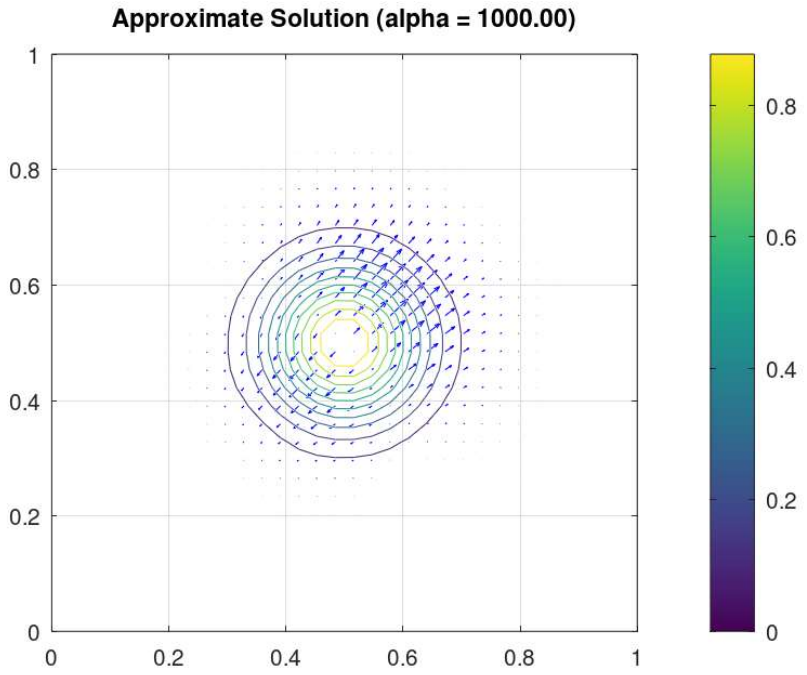

Figure 1: Approximate solution $u^h(x, y)$ with flux vectors for $\alpha = 10^3$

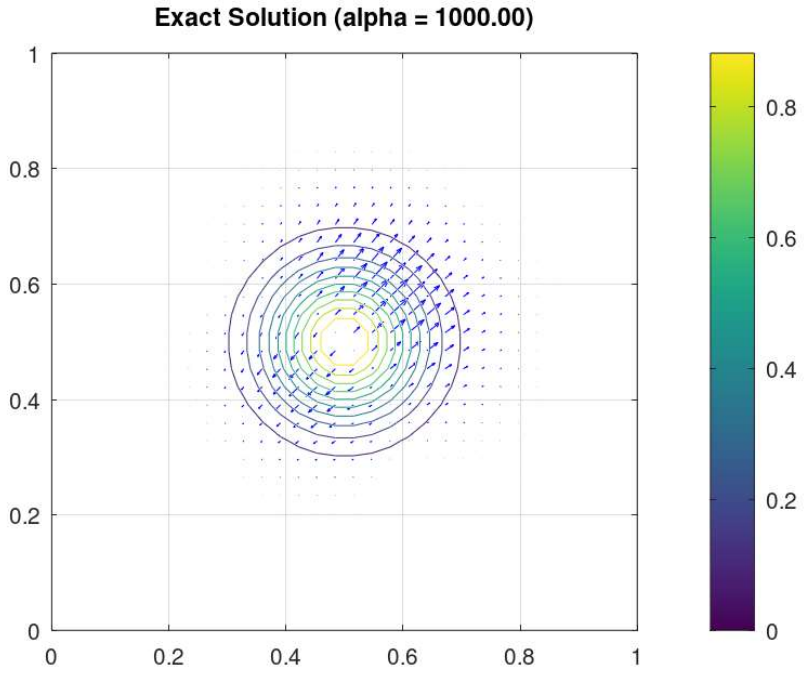

Figure 2: Manufactured exact solution $u(x, y)$ with flux vectors.

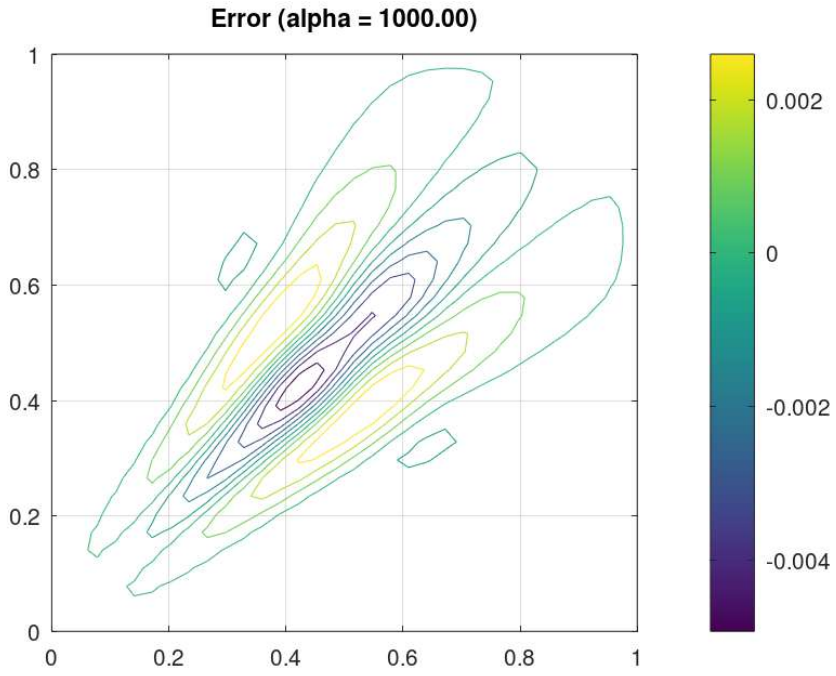

Figure 3: Pointwise error $u^h - u$.

6 Discussion

The main numerical difficulty in this problem was not the diagonal tensor terms, but the mixed x-y coupling induced by the off-diagonal conductivity entries. When $\alpha = 1$, these mixed terms vanish, so an incorrect implementation can appear to work. As α increases, however, the coupling becomes stronger, and errors in the staggered-grid assembly produce visible nonphysical artifacts.

The corrected implementation resolved this issue by distinguishing x-face and y-face locations explicitly, evaluating tensor coefficients on the appropriate face families, and introducing transfer operators for the off-diagonal blocks. Once this was done, both the scalar solution and the fluxes converged cleanly under refinement.

These results indicate that the mimetic framework is well suited to heterogeneous Darcy flow with full-tensor conductivity. The flux-divergence construction preserves the geometric structure of the continuous operator and provides a natural setting for conservative discretization on staggered grids.

7 Conclusion

In this investigation, a MOLE-based mimetic solver was implemented for a two-dimensional Darcy equation with heterogeneous anisotropic full-tensor conductivity. A manufactured exact solution was used to derive the forcing term and Dirichlet boundary data, allowing direct verification of both the scalar potential and the fluxes.

The key implementation issue was the correct discrete treatment of the mixed tensor terms on staggered face grids. After assembling these terms with face-specific sampling and

transfer operators, the method produced stable solutions and strong convergence for all tested anisotropy values.

The error tables and contour plots validate the implementation and show that mimetic differences provide an effective framework for full-tensor Darcy problems on staggered grids.

References

[1] J. E. Castillo and R. Grone, *A matrix analysis approach to higher-order approximations for divergence and gradient operators*, SIAM Journal on Matrix Analysis and Applications, 25 (2003), pp. 128–142.

[2] J. Corbino and J. E. Castillo, *High-order mimetic difference operators on staggered grids.* Technical Report CSRCR2024-09, Computational Science Research Center, San Diego State University, December 2024.

[3] J. Corbino, M. Dumett, and J. E. Castillo, *MOLE: Mimetic Operators Library Enhanced*, Journal of Open Source Software, vol. 9, no. 99, p. 6288, Jul. 2024, doi: 10.21105/joss.06288.

[4] MOLE Library (Mimetic Operators Library Enhanced), Computational Science Research Center, San Diego State University. Available at: https://github.com/csrc-sdsu/mole

[5] L. Traverso, T.N. Phillips, Y. Yang, *Mixed finite element methods for groundwater flow in heterogeneous aquifers*, Computers & Fluids, Volume 88, 2013, Pages 60-80,ISSN 0045-7930, https://doi.org/10.1016/j.compfluid.2013.08.018.